



## Site M0102<sup>1</sup>

### Contents

- 1 Operations
- 2 Lithostratigraphy
- 7 Physical properties
- 10 Geochemistry
- 13 Paleomagnetism
- 14 Geochronology
- 15 References

### Keywords

International Ocean Discovery Program, IODP, Expedition 389, *MMA Valour*, Hawaiian Drowned Reefs, Earth climate system, Earth system feedbacks, Earth history tipping points, Site M0102, coral reef, volcanics, sea level, paleoclimate, central Pacific, reef health, Hawaiian geology, basalt, lava, carbonates, Kohala

### Core descriptions

### Supplementary material

### References (RIS)

#### MS 389-109

Published 26 February 2025

Funded by ECORD, JAMSTEC, and NSF OCE1326927

J.M. Webster, A.C. Ravelo, H.L.J. Grant, M. Rydzy, M. Stewart, N. Allison, R. Asami, B. Boston, J.C. Braga, L. Brenner, X. Chen, P. Chutcharavan, A. Dutton, T. Felis, N. Fukuyo, E. Gischler, S. Greve, A. Hagen, Y. Hamon, E. Hathorne, M. Humblet, S. Jorry, P. Khanna, E. Le Ber, H. McGregor, R. Mortlock, T. Nohl, D. Potts, A. Prohaska, N. Prouty, W. Renema, K.H. Rubin, H. Westphal, and Y. Yokoyama<sup>2</sup>

<sup>1</sup>Webster, J.M., Ravelo, A.C., Grant, H.L.J., Rydzy, M., Stewart, M., Allison, N., Asami, R., Boston, B., Braga, J.C., Brenner, L., Chen, X., Chutcharavan, P., Dutton, A., Felis, T., Fukuyo, N., Gischler, E., Greve, S., Hagen, A., Hamon, Y., Hathorne, E., Humblet, M., Jorry, S., Khanna, P., Le Ber, E., McGregor, H., Mortlock, R., Nohl, T., Potts, D., Prohaska, A., Prouty, N., Renema, W., Rubin, K.H., Westphal, H., and Yokoyama, Y., 2025. Site M0102. In Webster, J.M., Ravelo, A.C., Grant, H.L.J., and the Expedition 389 Scientists, Hawaiian Drowned Reefs. Proceedings of the International Ocean Discovery Program, 389: College Station, TX (International Ocean Discovery Program).  
<https://doi.org/10.14379/iodp.proc.389.109.2025>

<sup>2</sup>Expedition 389 Scientists' affiliations.

## 1. Operations

The multipurpose vessel *MMA Valour* was used as the drilling platform throughout Expedition 389. At all Expedition 389 sites, dynamic positioning was used to provide accurate positions throughout operations and water depth was established using a Sound Velocity Profiler (SVP) placed on the top of the PROD5 drilling system. For more detail on acquisition methods, see **Introduction** in the Expedition 389 methods chapter (Webster et al., 2025a).

Summary operational information for Site M0102 is provided in Table **T1**. All times stated are in Hawaiian Standard Time (HST).

### 1.1. Hole M0102A

The *MMA Valour* arrived on location at 2100 h on 3 October 2023. PROD5 was deployed at 2308 h, and rotary coring and casing began in Hole M0102A at 0039 h on 4 October at a water depth of 412.8 m. Coring continued until a total hydraulic failure at 26.07 meters below seafloor (mbsf) meant Hole M0102A was abandoned at 1733 h, leaving 23 m of drill string and 8 m of casing in the seabed. PROD5 was recovered to deck at 1952 h on 4 October. On-deck operations commenced, and core barrels were extracted for curation. The transit back to Site M0101 was initiated at 0031 h on 5 October.

A total of 14 cores were recovered from Hole M0102A from 25.14 m of rotary coring. A total recovered core length of 11.08 m was achieved (44.07% recovery).

**Table T1.** Hole summary, Site M0102. R = rotary coring mode, W = wash down mode. LAT = Lowest Astronomical Tide. [Download table in CSV format.](#)

Hole	Water depth (mbsf)	Date started (2023)	Date finished (2023)	Latitude	Longitude	Coring method	Total drilled depth (m)	Recovered length (m)	Core recovery (%)	Cores (N)	Notes
389-M0102A	412.8	04 Oct	04 Oct	20.289983°	-155.650868°	R	25.14	11.08	44	14	LAT water depth: 412.4 m. Borehole abandoned due to technical issues. RC15 not recovered.
M0102B	415.4	08 Oct	08 Oct	20.289949°	-155.650948°	W	4.70	0	0	1	LAT water depth: 415.0 m. Wash only to 4.70 m. Borehole abandoned due to technical issues, no core recovery.
M0102C	415.9	08 Oct	11 Oct	20.289871°	-155.651009°	W, R	73.44	42.32	79	33	LAT water depth: 415.5 m. Wash to 19.90 m. Maximum number of barrels used.

### 1.2. Hole M0102B

The *MMA Valour* returned to Site M0102 at 1700 h on 7 October 2023. PROD5 was launched at 2256 h, and wash boring and casing commenced in Hole M0102B at 0018 h on 8 October at a water depth of 415.4 m. A crack in the manifold and subsequent sensor fault meant the hole was abandoned at 0149 h at 4.70 mbsf. PROD 5 was recovered to deck at 0249 h, and repairs commenced.

No core was recovered for Hole M0102B.

### 1.3. Hole M0102C

Following repairs, PROD5 was redeployed at 0744 h on 8 October 2023 at a water depth of 415.9 m. Coring in Hole M0102C commenced by wash boring and casing to 19.90 mbsf by 1747 h, just above the final depth of coring in Hole M0102A. Rotary coring commenced, and coring continued throughout 9 and 10 October to a final depth of 73.44 mbsf at 1159 h on 11 October after utilizing all drill barrels. PROD5 was recovered to deck by 1256 h, and on-deck operations commenced with core barrel extraction and on-deck curation. The transit to Site M0103 was underway at 1300 h on 11 October.

A total of 33 cores were recovered from Hole M0102C from 53.55 m of rotary coring and 19.89 m of wash boring. The total length of core recovered was 42.32 m (79.03% recovery).

## 2. Lithostratigraphy

Holes M0102A and M0102C are located in the Kohala region at 412.8 and 415.9 meters below sea level (mbsl), respectively. Based on the main facies changes and discontinuity surfaces, four main intervals are identified (Figure F1):

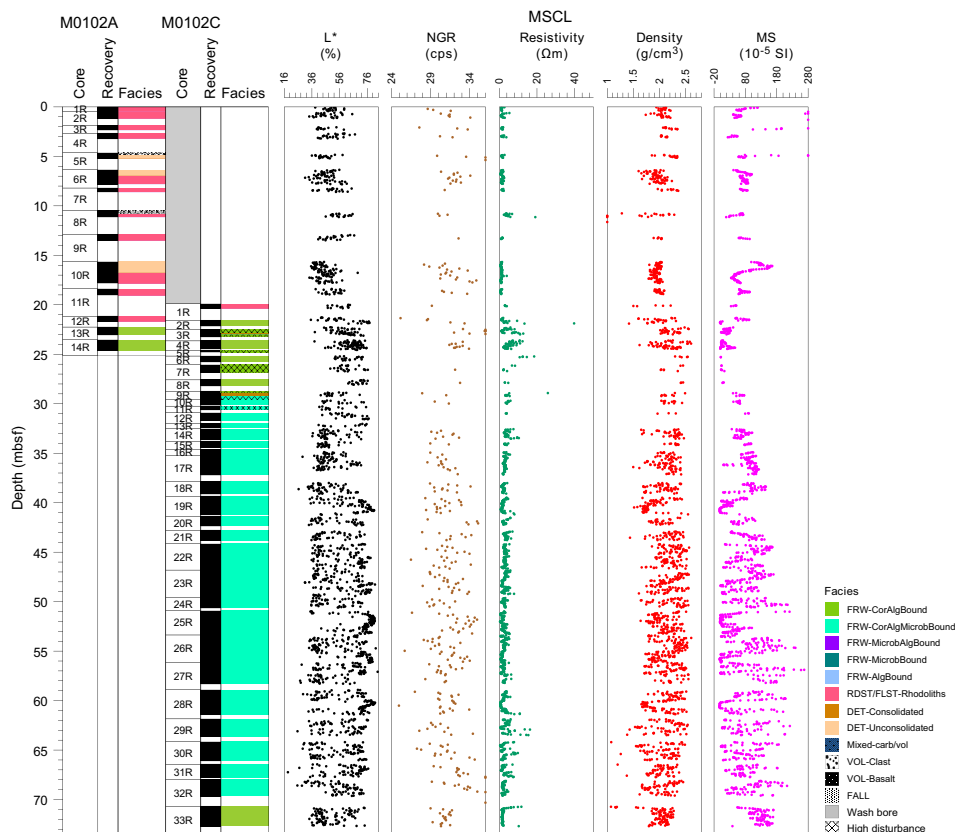


Figure F1. Composite lithostratigraphy, Holes M0102A and M0102C. cps = counts per second, MS = magnetic susceptibility.

- Interval 1 (0.00–22.25 mbsf) forms the major part of the core from Hole M0102A and consists of rhodoliths embedded in unconsolidated biotrital-volcaniclastic sediment. The basal boundary corresponds to a major facies change in both holes (M0102A and M0102C).
- Interval 2 (22.25–24.61 mbsf in Hole M0102A; 21.58–28.85 mbsf in Hole M0102C) is dominated by coralgall boundstone with submassive to massive *Porites*. It is bounded at its base by a thin layer of biotrital, coarse-grained grainstone to rudstone.
- Interval 3 (29.25–70.69 mbsf in Hole M0102C; not recovered in Hole M0102A) is a succession of in situ coralgall-microbialite boundstone with the genus changing downhole from branching and platy *Porites* and columnar *Pavona* to predominantly very large massive *Porites* with rare laminar *Pavona*.
- Interval 4 (70.69–72.71 mbsf in Hole M0102C; not recovered in Hole M0102A) consists of a coralgall boundstone with abundant branching and platy *Porites*.

## 2.1. Holes M0102A and M0102C

Holes M0102A and M0102C represent a composite hole and are described together (Figure F1). Cores from Hole M0102A span 0.00 to 24.61 mbsf (Figure F2). Hole M0102C was wash bored through most of the Hole M0102A interval and then rotary cored from 19.90 to 72.71 mbsf (Figure F3).

The lithology of Hole M0102A from 0.00 to 22.25 mbsf is composed of a relatively homogeneous facies comprising centimeter-sized rhodoliths embedded in unconsolidated biotrital sediment (Figure F4A). Bioclasts include bivalves, gastropods (*Polinices*), fragments of branching corals (rare Agariciidae), and crustose coralline algae (CCA) crusts, bryozoan branches, and large benthic foraminifers (LBFs). In the lower part of this interval, from 16.75 to 22.25 mbsf, coral fragments are more diverse and include pieces of *Cyphastrea* and *Leptoseris* (Figure F4B) and one occurrence of *Diaseris* (free-living coral). The sand fraction contains bioclasts and fine- to medium-grained volcaniclastic sediments with rare black volcanic granules. Rhodoliths are predominantly composed of CCA encrustations with vermetids, encrusting foraminifers (*Homotrema*), and bryozoans, with some bryozoan and coral fragments acting as rhodolith nuclei.

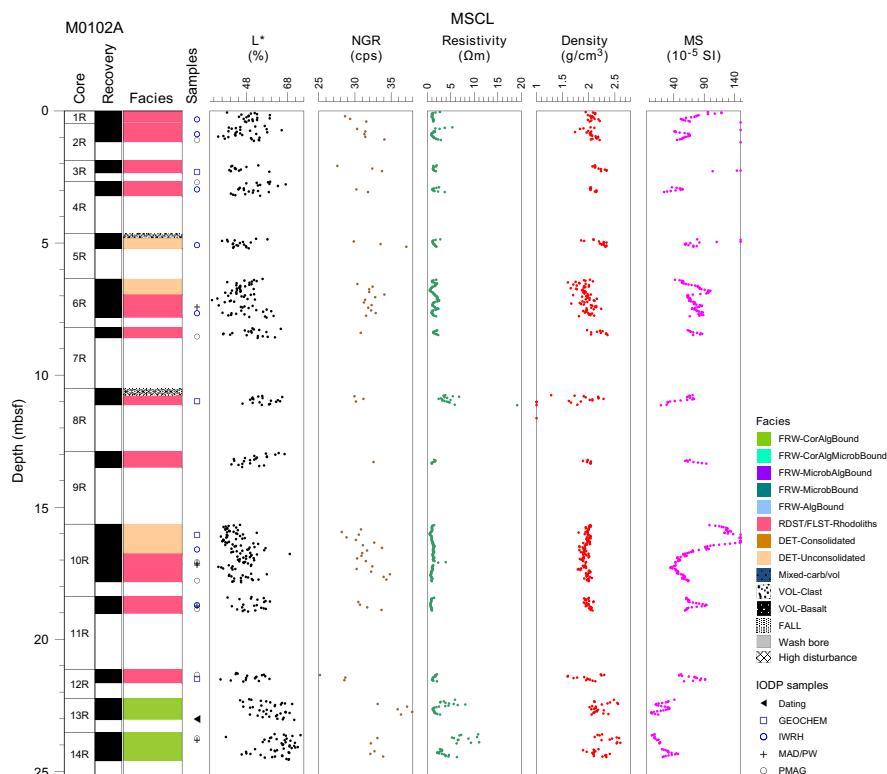


**Figure F2.** Lithostratigraphy and MSCL data, Hole M0102A. cps = counts per second, MS = magnetic susceptibility.

The rhodolith-rich facies is interrupted by two intervals of unconsolidated biodetrital sediment, from 4.64 to 6.95 mbsf and from 15.64 to 16.75 mbsf, that are devoid of rhodoliths (Figure F4C). These sediments are composed of LBFs, gastropod shells (*Cypraea*), coral fragments (*Leptoseris*, *Cyphastrea*, and branching *Montipora*), CCA fragments, and fine- to medium-grained volcaniclastic sand with rare black volcanic granules.

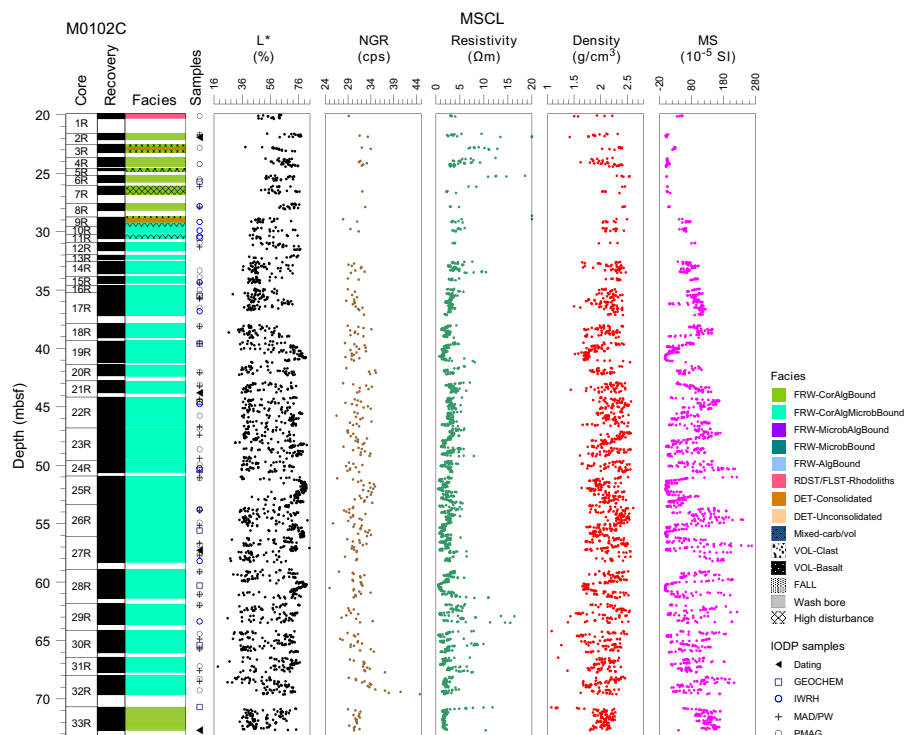


**Figure F3.** Lithostratigraphy and MSCL data, Hole M0102C. cps = counts per second, MS = magnetic susceptibility.

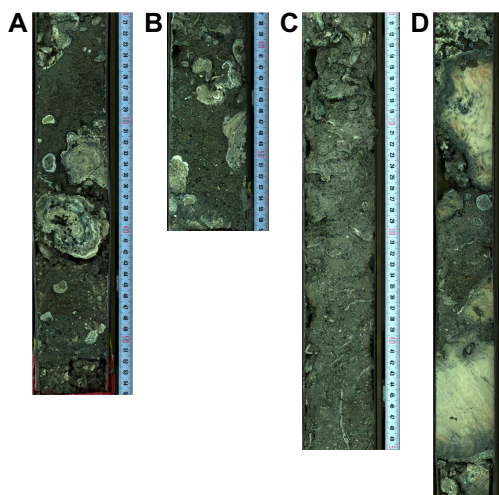


**Figure F4.** Facies, Hole M0102A. A. Rhodolith-rich facies composed of centimeter-sized rhodoliths embedded in unconsolidated biodetrital sediment (4R-1, 20–55 cm). B. Rhodolith-rich facies containing coral fragments including pieces of *Cyphastrea* and *Leptoseris* (11R-1, 37–57 cm). C. Unconsolidated biodetrital sediment containing LBFs, gastropod shells (*Cypraea*), coral fragments (*Leptoseris*, *Cyphastrea*, and branching *Montipora*), CCA fragments, and a fine- to medium-grained volcaniclastic sandy fraction (6R-1, 10–50 cm). D. Coralgal boundstone consisting of large pieces of heavily bored, massive *Porites* with stained margins and CCA crusts (13R-1, 7–65 cm). Corals are embedded in an unconsolidated biodetrital and volcaniclastic matrix with rare centimeter-sized rhodoliths.

From 22.25 to 24.61 mbsf, a fragmented (due to core disturbance) coralgall boundstone consists of large pieces of strongly bioeroded massive *Porites* with surface staining that are encrusted with CCA with bryozoans and vermetids (Figure F4D). Rare centimeter-sized rhodoliths are observed. The coarse components are embedded in an unconsolidated biodetrital and volcaniclastic matrix similar to that observed above.

The sedimentary succession continues downward in Hole M0102C from 19.90 to 72.71 mbsf, with approximately 5 m overlap with Hole M0102A (Figure F3).

From 19.90 to 21.58 mbsf, the core consists of centimeter-sized rhodoliths composed of laminar and fruticose coralline algae (FCA), bryozoans, and encrusting foraminifers; some rhodoliths reveal coral nuclei (Figure F5A). These rhodoliths are associated with fragments of *Cyphastrea*.

The interval from 21.58 to 28.85 mbsf consists of coralgall boundstone that is interlayered locally, between 22.77 and 23.01 mbsf, with biodetrital, coarse-grained rudstone with coral fragments (*Porites*, *Millepora*, and *Pocillopora*), bivalves, gastropods, and echinoid spines (Figure F5B). Most corals in the coralgall boundstone are submassive to massive *Porites* that show some dark growth bands, are in many cases bored (*Trypanites*), and are rarely encrusted with thin CCA crusts (Figure F6). Below 24.62 mbsf, the coral assemblage is more diverse and includes a few encrusting *Cyphastrea* and *Leptastrea*, foliaceous *Leptoseris*, and encrusting *Montipora* in order of declining abundance (Figure F7A).

The interval from 28.85 to 29.25 mbsf represents a transition between the facies above and below and is composed of biodetrital, coarse-grained rudstone to grainstone with coral fragments

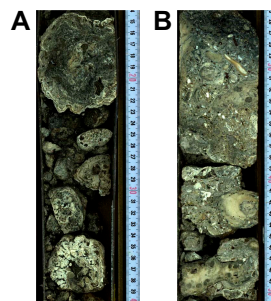


**Figure F5.** Facies, Hole M0102C. A. Rhodoliths composed of laminar and FCA, bryozoans, and encrusting foraminifers (1R-1, 14–40 cm). B. Coralgall boundstone interlayered locally by biodetrital, coarse-grained rudstone with coral fragments (*Porites*, *Millepora*, and *Pocillopora*), bivalves, gastropods, and echinoid spines (3R-1, 25–51 cm).

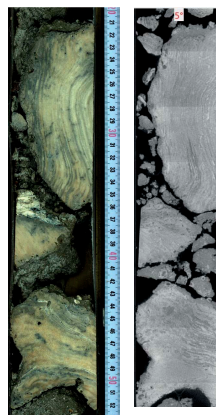


**Figure F6.** Lithology, Hole M0102C. Coralgall boundstone of submassive to massive *Porites* showing some dark growth bands and rare thin CCA crusts (4R-1, 20–53 cm). Left: high-resolution linescan image. Right: X-ray computed tomography scan image (orthogonal view 0°–180°).

(*Porites*, *Leptoseris*, *Millepora*, and *Cyphastrea*) in a bioclastic matrix (algal debris, gastropods, and bivalves) (Figure F7B).

Below this transitional interval, the lithology from 29.25 to 70.69 mbsf consists of in situ coralgal-microbialite boundstone composed of corals with thin CCA crusts with vermetids and *Homotrema* as well as thick massive to dendritic microbialite crusts with structureless to thrombotic internal fabric (Figure F8). Echinoid spines (*Heterocentrotus*) are embedded in the microbialite. Framework cavities are filled with unconsolidated, fine-grained, dark sediment of mixed biotrital and volcanoclastic material. From 29.25 to 37.86 mbsf, branching and platy *Porites* and columnar *Pavona* occur (Figure F9A) along with a few encrusting *Cyphastrea* and platy *Leptoseris*. From 37.86 to 70.69 mbsf, corals are predominantly very large massive *Porites* (up to 1.5 m thick) (Figure F9B) with rare laminar *Pavona* (only between 44.16 and 46.79 mbsf), encrusted with thick, heavily bored CCA crusts with vermetid tubes (Figure F9C) and locally associated with encrusting *Cyphastrea*.

At the base of Hole M0102C, a coralgal boundstone from 70.69 to 72.71 mbsf consists of numerous branching and platy *Porites* covered with thin CCA crusts (encrusting some vermetids) and locally by very thin microbialite crusts embedded in a matrix of abundant, patchily consolidated, medium- to coarse-grained volcanoclastic and biotrital clasts (Figure F10A). Both corals and CCA crusts are diagenetically altered. Two oxidized (millimeter-thick) crusts at 71.39 and 72.38 mbsf are observed on top of consolidated sediments (Figure F10B).

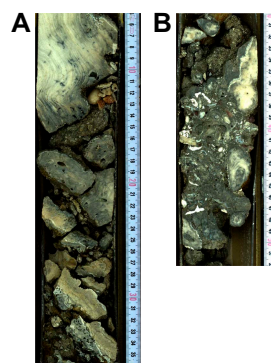


**Figure F7.** Coral, Hole M0102C. A. Coral assemblage comprising *Porites* with encrusting *Cyphastrea* and *Leptastrea*, foliaceous *Leptoseris*, and encrusting *Montipora* (7R-1, 5–36 cm). B. Biotrital, coarse-grained rudstone to grainstone with coral fragments (*Porites*, *Leptoseris*, *Millepora*, and *Cyphastrea*) in a bioclastic matrix of algal debris, gastropods, and bivalves located at the transition between lithostratigraphic Intervals 2 and 3 (9R-1, 30–52 cm).

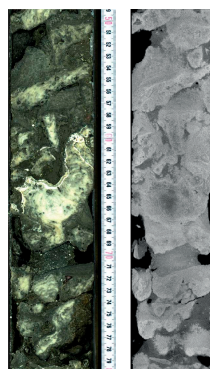


**Figure F8.** Lithologies, Hole M0102C. Coralgal-microbialite boundstone of corals with thin CCA crusts (with vermetid tubes and *Homotrema*) and thick massive to dendritic microbialite crusts with structureless to thrombotic internal fabric (14R-1, 49–80 cm). Left: high-resolution linescan image. Right: X-ray computed tomography scan image (orthogonal view 0°–180°).

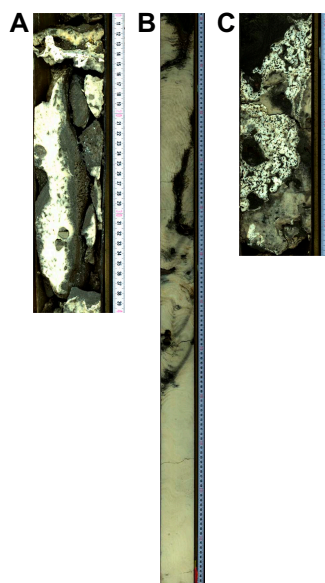


**Figure F9.** *Porites* and vermetids, Hole M0102C. A. Branching and platy *Porites* and columnar *Pavona* (12R-1, 10–40 cm). B. Very large massive *Porites* (19R-1, 29–150 cm). C. Thick, heavily bored algal crust with vermetids (24R-1, 79–103 cm).

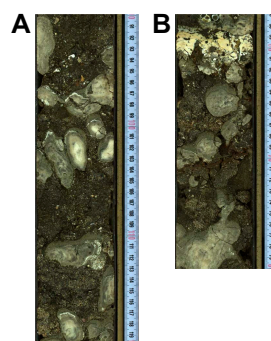


**Figure F10.** Crusts, Hole M0102C. A. Branching and platy *Porites* with thin CCA crusts and rare very thin microbialite crusts embedded in a matrix of abundant, patchily consolidated, medium- to coarse-grained volcaniclastic and biodetrital clasts (33R-1, 90–120 cm). B. Millimeter-thick oxidized crust (at 70 cm) above consolidated, medium- to coarse-grained volcaniclastic and biodetrital sediments (33R-1, 57–80 cm).

## 2.2. Hole M0102B

This hole was cored by wash bore only; no core was recovered (Table T1).

## 3. Physical properties

Physical properties data for Site M0102 are shown in Table T2 in the Site M0096 chapter (Webster et al., 2025b).

### 3.1. Hole M0102A

A total of 11.01 m of core from Hole M0102A was scanned with the multisensor core logger (MSCL), and because the core exhibited only minor drilling-induced disturbance, 75% of the acquired data passed QA/QC (see Table T10 in the Expedition 389 methods chapter [Webster et al., 2025a]). A total of five discrete samples were used for *P*-wave and moisture and density (MAD) measurements. Digital linescans, color reflectance, and hyperspectral imaging were acquired on all cores.

### 3.1.1. Density and porosity

Data for density and porosity measurements are presented in Figures F2 and F11. MSCL bulk density measurements range 0.69–2.60 g/cm<sup>3</sup>. A total of five discrete samples, including four sediment plugs, were analyzed for MAD, giving bulk density values in the range of 1.82–2.35 g/cm<sup>3</sup>. Porosity values for the same samples range 27.4%–53.7%, and grain density values fluctuate between 2.669 and 2.864 g/cm<sup>3</sup>. An increase in bulk density occurs at the base of the core in both the MSCL and discrete sample data and corresponds to a change in lithology from rudstone/floatstones (rhodoliths) to coralgal-microbialite boundstone (see [Lithostratigraphy](#)).

### 3.1.2. P-wave velocity

MSCL *P*-wave velocity measurements yielded no data. One sample was measured using the discrete *P*-wave logger. This sample has a dry velocity of 4078 m/s and a resaturated velocity of 4149 m/s (Figure F12).

### 3.1.3. Thermal conductivity

Because of the presence of drilling-induced disturbance damage, large voids, and uneven surfaces, thermal conductivity measurements were not performed on Hole M0102A cores.

### 3.1.4. Magnetic susceptibility

MSCL magnetic susceptibility data range  $2.55 \times 10^{-5}$  to  $1290.01 \times 10^{-5}$  SI (Figures F1, F2). The majority of magnetic susceptibility values fall close to  $86.62 \times 10^{-5}$  SI. High variations are found throughout the hole, with the largest variability near the top of Core 389-M0102A-10R relative to the base of the hole.

### 3.1.5. Electrical resistivity

MSCL noncontact resistivity measurements yielded data ranging 0.52–19.12 Ωm (Figures F1, F2). Little variation is generally found except at the base of the hole, where values are relatively high.

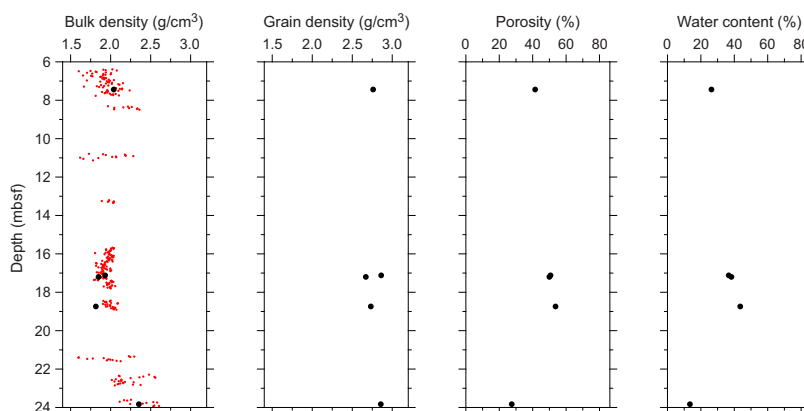


**Figure F11.** Physical properties, Hole M0102A. Black = discrete samples, red = MSCL.

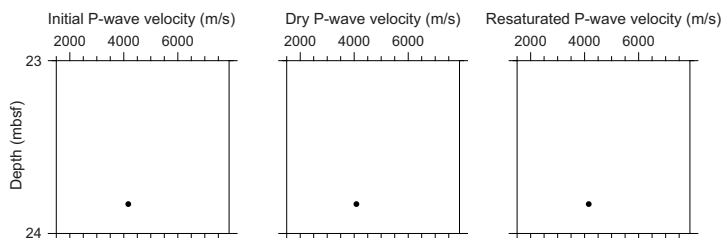


**Figure F12.** Initial, dry, and resaturated *P*-wave velocities measured on one discrete sample, Hole M0102A.



### 3.1.6. Natural gamma radiation

MSCL natural gamma radiation (NGR) measurements range 25–38 counts/s (Figures F1, F2), showing no apparent downhole change.

### 3.1.7. Digital linescans, color reflectance, and hyperspectral imaging

All cores were digitally scanned, measured for color reflectance (where appropriate), and imaged with the hyperspectral scanner (see HYPERSPECTRAL in Supplementary material). Color reflectance  $L^*$  values vary between 31.08% and 74.35%,  $a^*$  varies between  $-1.31$  and  $5.33$ ,  $b^*$  varies between 2.17 and 20.07, and  $a^*/b^*$  varies between  $-0.43$  and  $0.31$  (Figures F1, F2).

## 3.2. Hole M0102B

This hole was cored by wash bore only; no core was recovered (Table T1).

## 3.3. Hole M0102C

A total of 42.13 m of core from Hole M0102C was scanned with the MSCL, and because the core exhibited only minor drilling-induced disturbance, 75% of the acquired data passed QA/QC (see Table T10 in the Expedition 389 methods chapter [Webster et al., 2025a]). A total of 27 discrete samples for  $P$ -wave and MAD measurements, as well as digital linescans, color reflectance, and hyperspectral imaging, were acquired on all core sections.

### 3.3.1. Density and porosity

Data for density and porosity measurements are presented in Figures F2 and F13. MSCL bulk density measurements range  $1.08$ – $2.61$   $\text{g}/\text{cm}^3$  (Figures F1, F3). A total of 27 discrete samples were analyzed for MAD, and bulk density values range  $1.75$ – $2.64$   $\text{g}/\text{cm}^3$ , in contrast to MSCL density values. Porosity values for the same samples range 10.6%–60.7%, and grain density values range  $2.294$ – $2.907$   $\text{g}/\text{cm}^3$ . There are no clear downhole trends in the density and porosity data sets and no clear relationship between the two bulk density measurements (MSCL and discrete).

### 3.3.2. $P$ -wave velocity

MSCL  $P$ -wave velocity measurements yielded no data. A total of 27 samples were measured using the discrete  $P$ -wave logger. Dry measurement values are between 3183 and 5229 m/s (Figure F14).  $P$ -wave velocity recorded for the samples after resaturation range 3066–5253 m/s. There are no apparent downhole trends.

### 3.3.3. Thermal conductivity

Thermal conductivity was collected on two cores. A value of  $1.450$   $\text{W}/(\text{m}\cdot\text{K})$  was recorded at 48.39 mbsf, and  $1.388$   $\text{W}/(\text{m}\cdot\text{K})$  was recorded at 51.06 mbsf (see Table T11 in the Expedition 389 methods chapter [Webster et al., 2025a]).

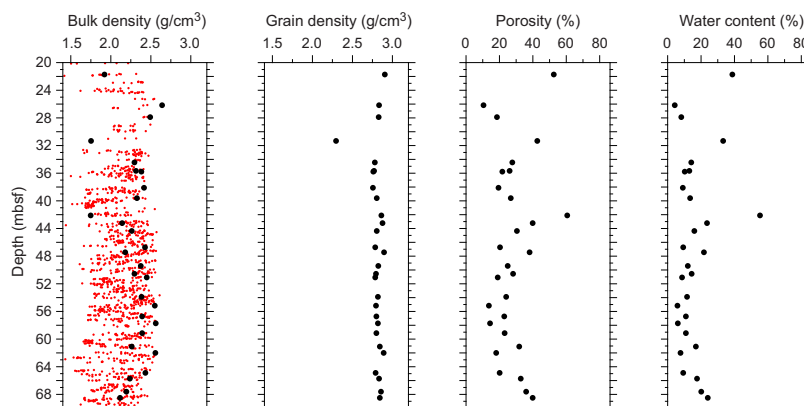
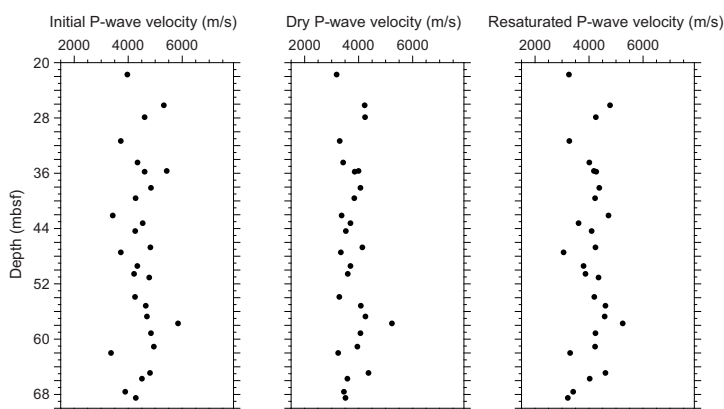


Figure F13. Physical properties, Hole M0102C. Black = discrete samples, red = MSCL.



**Figure F14.** Initial, dry, and resaturated *P*-wave velocities measured on discrete samples, Hole M0102C.

### 3.3.4. Magnetic susceptibility

MSCL magnetic susceptibility data range  $-1.68 \times 10^{-5}$  to  $267.75 \times 10^{-5}$  SI (Figures F1, F3) with mean values close to  $74.75 \times 10^{-5}$  SI. The top of Core 389-M0102C-10R ( $\sim 15.5$  mbsf) shows higher than mean values with a change to lower than mean values occurring at  $\sim 16.5$  mbsf and may reflect the lithology change from unconsolidated biotrital sediment to a rhodolith floatstone. The lowest values are found below 22 mbsf. The high variability in Interval 3 (see Lithostratigraphy) below 40 mbsf occurs where abundant microbialites incorporate significant volumes of pyroxene (see Geochemistry).

### 3.3.5. Electrical resistivity

MSCL noncontact resistivity measurements range 0.46–39.82  $\Omega\text{m}$  (Figures F1, F3).

### 3.3.6. Natural gamma radiation

MSCL NGR measurements range 25–45 counts/s (Figures F1, F3), showing the largest values near the boundary between Interval 3 and Interval 4 (70.69 mbsf) at the base of Core 389-M0102C-32R.

### 3.3.7. Digital linescans, color reflectance, and hyperspectral imaging

All cores were digitally scanned, and, where appropriate, cores were measured for color reflectance and imaged with the hyperspectral scanner (see HYPERSPECTRAL in Supplementary material). Color reflectance  $L^*$  values vary between 18.72% and 83.57%,  $a^*$  varies between  $-1.57$  and 7.17,  $b^*$  varies between 1.75 and 28.11, and  $a^*/b^*$  varies between  $-0.30$  and 0.87 (Figures F1, F3). High variations in color reflectance parameters are found throughout the core, particularly in Interval 3 (29.25–70.69 mbsf) where abundant dark-colored microbialites are present.

## 4. Geochemistry

### 4.1. Interstitial water

A total of 14 interstitial water samples were collected from Site M0102 (7 from Hole M0102A and 7 from Hole M0102C). Of these, 12 samples were analyzed for salinity and ammonium concentration and 10 samples were analyzed for pH and alkalinity while off shore. Major cations and anions of seven samples were measured during the Onshore Science Party (see Table T16 in the Expedition 389 methods chapter [Webster et al., 2025a]). After combining samples from Holes M0102A and M0102C as a composite section, the pH data show a downcore trend to lower values with  $R^2 = 0.69$  ( $p$ -value  $< 0.005$ ; Figure F15). High ammonium concentrations were measured in Samples 389-M0102A-2R-1, 40 cm (95.4  $\mu\text{mol/L}$ ), and 4R-1, 30 cm (85.9  $\mu\text{mol/L}$ ), from 0.88 and 2.97 mbsf, respectively. Sample 1R-1, 32 cm (0.32 mbsf), has a high alkalinity of 17.64 mmol/L; however, the pH and salinity of this sample remain within range of other samples from Expedition 389, indicat-

ing a potential analytical error for this alkalinity measurement. Sample 389-M0102C-22R-1, 59.5 cm (44.80 mbsf), has the lowest alkalinity value measured during this expedition: 1.81 mmol/L (Figure F15).

Results show that some samples have elevated amounts of B, Ba, Si, and Sr compared to seawater (see Tables T15 and T17 in the Expedition 389 methods chapter [Webster et al., 2025a]). Calcium shows a downhole trend toward higher values, and Sr also increases with depth, peaking at around 45 mbsf, whereas Si shows the opposite trend. Manganese is above detection limit from 28 mbsf downcore (Figure F16).

### 4.2. Surface seawater

One surface seawater sample was collected from Site M0102 using a Niskin bottle deployed from the side of the vessel (see Figure F22 in the Expedition 389 methods chapter [Webster et al., 2025a]). Parameters including salinity, pH, alkalinity, and concentrations of ammonium were analyzed off shore, and major cations and anions were measured during the Onshore Science Party. The salinity, pH, alkalinity, and ammonium measured for this sample are consistent with the other surface seawater samples taken during Expedition 389 and align with the expected values for con-

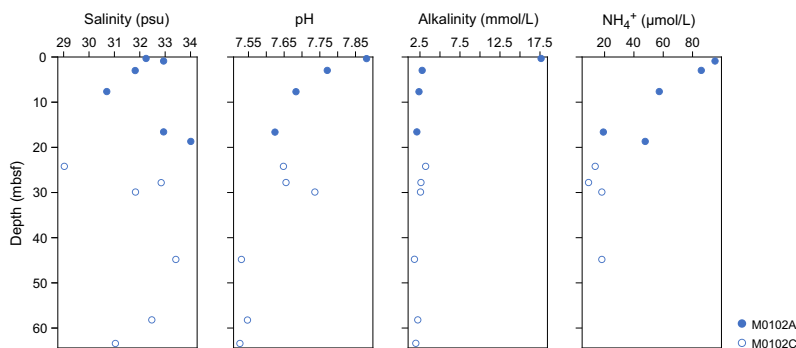


Figure F15. Interstitial water salinity, pH, alkalinity, and ammonium, Site M0102.

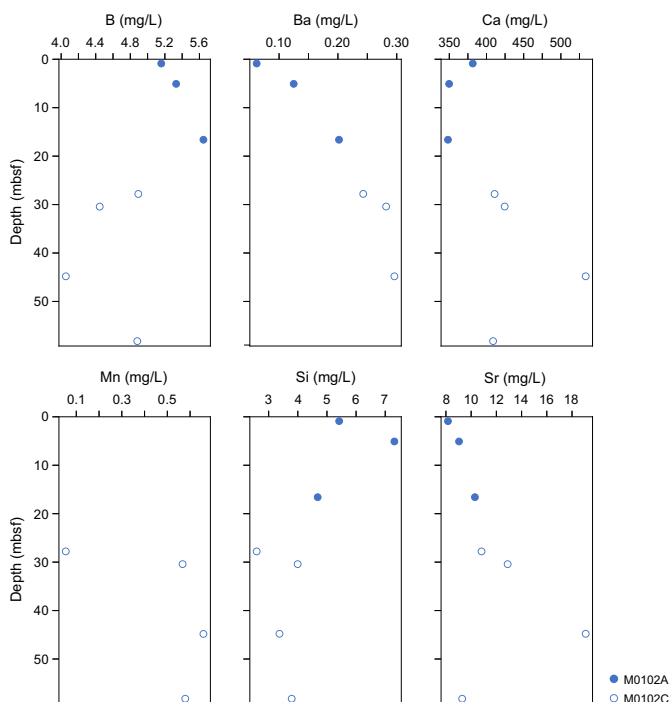


Figure F16. Interstitial water B, Ba, Ca, Si, Sr and Mn, Site M0102.

servative elements in seawater. Concentrations of K (412 mg/L), Mg (1306 mg/L), and Sr (7.6 mg/L) are the highest measured during this expedition (see Tables **T15** and **T16** in the Expedition 389 methods chapter [Webster et al., 2025a]).

### 4.3. Bulk sediment

A total of 14 bulk sediments were taken from Site M0102 (Figure **F2**) and analyzed for mineralogy, elemental composition, and carbon content. Samples are derived from a variety of facies (see Figure **F10** in the Expedition 389 methods chapter [Webster et al., 2025a]), including rhodoliths, unconsolidated sediment, coralgall boundstone, and coralgall-microbialite boundstone (Figures **F2**, **F7**).

### 4.4. Mineralogy

Samples from Site M0102 are mostly composed of the carbonate minerals aragonite, high-Mg calcite, and  $\leq 10\%$  calcite, except for the sample from the coralgall boundstone at 70.70 mbsf (Sample 389-M0102C-33R-1, 1–3 cm), which contains 56% calcite (Table **T2**). The X-ray diffraction results suggest Sample 30R-1, 123–125 cm, contains 18% manganocalcite or related manganese-rich carbonates. Other minerals detected in the samples include quartz, cristobalite, plagioclase (up to 12%), gypsum and related minerals, apatite and other phosphate minerals, kaolinite, spinel magnetite, aluminum oxides, and sulfides. Samples from the coralgall-microbialite boundstone at 35.50 and 39.60 mbsf (Samples 17R-1, 30–33 cm, and 19R-1, 27–29 cm) also contain 12% pyroxene.

### 4.5. Elemental abundances

Although the Ca concentration in the samples is high and stays mostly constant downhole at an average of 318,983 mg/kg, concentrations of the other major elements vary in bulk sediment and rock samples from Site M0102 (Table **T3**; Figure **F17**). Compared to the unit above, from 20 to 50 mbsf, where the lithology is dominated by coralgall and coralgall-microbialite boundstone (Figure **F2**), the chemistry is characterized by slightly higher Al, Fe, Mn, and Ti with lower Br. At 60 mbsf, within the coralgall-microbialite boundstone, concentrations for Al, Br, Fe, Mg, Mn, Si, and Ti are lower than in the unit above. Here, the Sr concentration is the highest at 6,498 mg/kg. Other elements analyzed are minor or below detection limit.

### 4.6. Carbon content

The results for total organic carbon (TOC), total carbon (TC), and total inorganic carbon (TIC) at Site M0102 are presented in Table **T4**. TC content ranges 10.0%–11.4%, TOC content ranges 0.13%–0.35%, and TIC content ranges 9.8%–11.3%. TOC is higher in the shallower Hole M0102A, dominated by rhodolith facies by about 0.06% and 0.2% compared to Hole M0102C, except for the deepest sample in Hole M0102C (33R-1, 1–3 cm), where the TOC increases to 0.23%.

**Table T2.** Mineral abundances, Site M0102. [Download table in CSV format.](#)

**Table T3.** Bulk elemental compositions, Site M0102. [Download table in CSV format.](#)

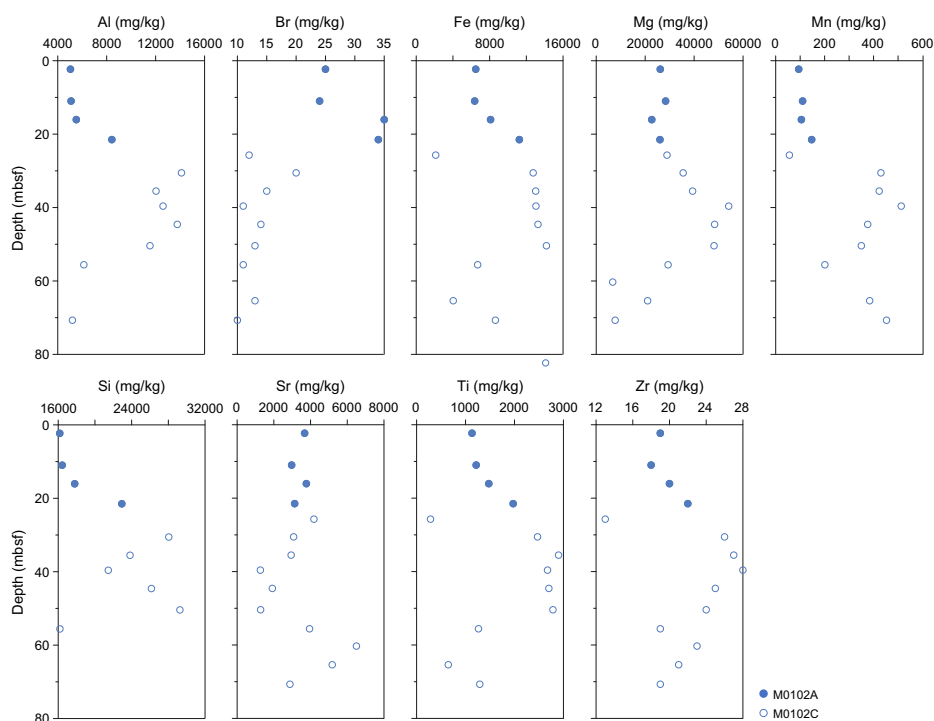


**Figure F17.** Bulk sediment and rock Al, Br, Fe, Mg, Mn, Si, Sr, Ti, and Zr, Site M0102.

**Table T4.** TOC, TC, and TIC, Site M0102. [Download table in CSV format.](#)

## 5. Paleomagnetism

A total of 38 plug samples and 3 cube samples were obtained from Holes M0102A and M0102C. Measurements of low-field and mass-specific magnetic susceptibility ( $\chi$ ) were carried out for all samples. Natural remanent magnetization (NRM) was measured for all plug samples, as well as remanence following stepwise alternating field (AF) demagnetization up to a peak AF of 20 mT and up to 100 mT for basalt samples. Cube samples were not demagnetized. For further details, see [Paleomagnetism](#) in the Expedition 389 methods chapter (Webster et al., 2025a).

### 5.1. Hole M0102A

Hole M0102A samples include volcanoclastic and bioclastic sediments, as well as other carbonate materials. Three cube samples were taken from 17.09, 17.79, and 18.87 mbsf in Hole M0102A; these samples consist of bioclastic sand, including a clast with volcanic material. The  $\chi$  values of the cube samples range  $4.50 \times 10^{-7}$  to  $7.24 \times 10^{-7}$  m<sup>3</sup>/kg with an arithmetic mean of  $5.97 \times 10^{-7}$  m<sup>3</sup>/kg. Five carbonate samples were also collected from Hole M0102A. Positive  $\chi$  values occur throughout, except for the sample at 23.76 mbsf (Sample 14R-1, 20.5–22.5 cm). Values range  $-0.22 \times 10^{-7}$  to  $16.2 \times 10^{-7}$  m<sup>3</sup>/kg with an arithmetic mean of  $9.87 \times 10^{-7}$  m<sup>3</sup>/kg. The initial NRM intensity values for 0 mT range  $0.0019 \times 10^{-1}$  to  $3.01 \times 10^{-1}$  A/m with an arithmetic mean of  $1.38 \times 10^{-1}$  A/m (Figure F18).

### 5.2. Hole M0102D

This hole was cored by wash bore only; no core was recovered (Table T1).

### 5.3. Hole M0102C

One lava sample (Sample 389-M0102C-30R-1, 27.5–29.5 cm) and 32 carbonate samples were taken from Hole M0102C. The  $\chi$  value of the lava sample is  $1.45 \times 10^{-5}$  m<sup>3</sup>/kg, and the initial NRM

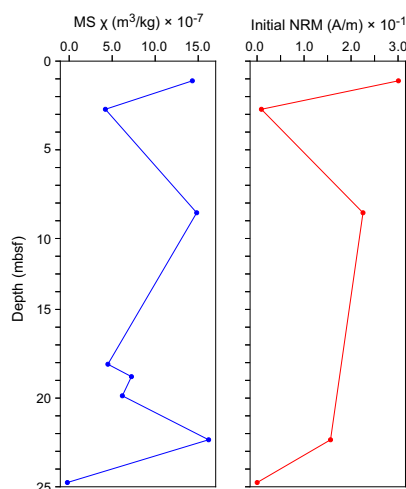


**Figure F18.** Magnetic susceptibility (MS) and NRM, Hole M0102A.

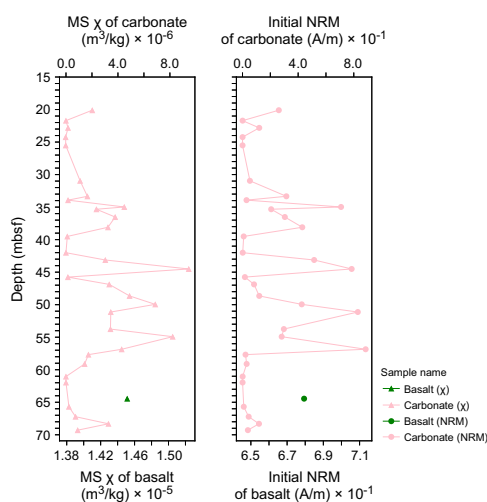


**Figure F19.** Magnetic susceptibility (MS) and NRM, Hole M0102C.

intensity is  $6.79 \times 10^{-1}$  A/m. The  $\chi$  values of carbonate samples range  $-0.026 \times 10^{-6}$  to  $9.45 \times 10^{-6}$   $\text{m}^3/\text{kg}$  with an arithmetic mean of  $2.32 \times 10^{-6}$   $\text{m}^3/\text{kg}$ . The initial NRM intensity values for 0 mT on the carbonate samples range  $0.0028 \times 10^{-1}$  to  $8.85 \times 10^{-1}$  A/m with an arithmetic mean of  $2.17 \times 10^{-1}$  A/m. Patterns in  $\chi$  and initial NRM are synchronous, suggesting that magnetic concentration and properties are the main drivers behind these variations (Figure F19).

## 6. Geochronology

Five U-Th dates were measured on samples from Site M0102, including one from Hole M0102A and four from Hole M0102C, spanning  $\sim 171$ – $225$  ky BP (see Tables T21 and T22 in the Expedition 389 methods chapter [Webster et al., 2025a]). None of these dates were rejected based on the U-Th geochemistry. However, in Hole M0102C there is one stratigraphic age reversal (Sample 27R-1, 115–117 cm). Overall, the dates from Site M0102 are consistent with the timing of development of the H2 terrace (Webster et al., 2009).

## References

- Webster, J.M., Braga, J.C., Clague, D.A., Gallup, C., Hein, J.R., Potts, D.C., Renema, W., Riding, R., Riker-Coleman, K., Silver, E., and Wallace, L.M., 2009. Coral reef evolution on rapidly subsiding margins. *Global and Planetary Change*, 66(1–2):129–148. <https://doi.org/10.1016/j.gloplacha.2008.07.010>
- Webster, J.M., Ravelo, A.C., Grant, H.L.J., and the Expedition 389 Scientists, 2025. Supplementary material, <https://doi.org/10.14379/iodp.proc.389supp.2025>. In Webster, J.M., Ravelo, A.C., Grant, H.L.J., and the Expedition 389 Scientists, Hawaiian Drowned Reefs. *Proceedings of the International Ocean Discovery Program, 389: College Station, TX (International Ocean Discovery Program)*.
- Webster, J.M., Ravelo, A.C., Grant, H.L.J., Rydzy, M., Stewart, M., Allison, N., Asami, R., Boston, B., Braga, J.C., Brenner, L., Chen, X., Chutcharavan, P., Dutton, A., Felis, T., Fukuyo, N., Gischler, E., Greve, S., Hagen, A., Hamon, Y., Hathorne, E., Humblet, M., Jorry, S., Khanna, P., Le Ber, E., McGregor, H., Mortlock, R., Nohl, T., Potts, D., Prohaska, A., Prouty, N., Renema, W., Rubin, K.H., Westphal, H., and Yokoyama, Y., 2025a. Expedition 389 methods. In Webster, J.M., Ravelo, A.C., Grant, H.L.J., and the Expedition 389 Scientists, Hawaiian Drowned Reefs. *Proceedings of the International Ocean Discovery Program, 389: College Station, TX (International Ocean Discovery Program)*. <https://doi.org/10.14379/iodp.proc.389.102.2025>
- Webster, J.M., Ravelo, A.C., Grant, H.L.J., Rydzy, M., Stewart, M., Allison, N., Asami, R., Boston, B., Braga, J.C., Brenner, L., Chen, X., Chutcharavan, P., Dutton, A., Felis, T., Fukuyo, N., Gischler, E., Greve, S., Hagen, A., Hamon, Y., Hathorne, E., Humblet, M., Jorry, S., Khanna, P., Le Ber, E., McGregor, H., Mortlock, R., Nohl, T., Potts, D., Prohaska, A., Prouty, N., Renema, W., Rubin, K.H., Westphal, H., and Yokoyama, Y., 2025b. Site M0096. In Webster, J.M., Ravelo, A.C., Grant, H.L.J., and the Expedition 389 Scientists, Hawaiian Drowned Reefs. *Proceedings of the International Ocean Discovery Program, 389: College Station, TX (International Ocean Discovery Program)*. <https://doi.org/10.14379/iodp.proc.389.103.2025>